

# Numerical Modeling of Land Subsidence Resulting from Oil Production

Zhang, S., Zhong, R., Liu, Y.

*The University of Tulsa, Tulsa, Oklahoma, USA*

Copyright 2016 ARMA, American Rock Mechanics Association

This paper was prepared for presentation at the 50<sup>th</sup> US Rock Mechanics / Geomechanics Symposium held in Houston, Texas, USA, 26-29 June 2016. This paper was selected for presentation at the symposium by an ARMA Technical Program Committee based on a technical and critical review of the paper by a minimum of two technical reviewers. The material, as presented, does not necessarily reflect any position of ARMA, its officers, or members. Electronic reproduction, distribution, or storage of any part of this paper for commercial purposes without the written consent of ARMA is prohibited. Permission to reproduce in print is restricted to an abstract of not more than 200 words; illustrations may not be copied. The abstract must contain conspicuous acknowledgement of where and by whom the paper was presented.

**ABSTRACT:** The oil production can cause land subsidence when large amounts of underground fluid have been withdrawn from geo-pressured reservoirs. In this paper, a fast-running numerical model coupled with production history is developed to calculate the land subsidence for arbitrary shape reservoirs. The model is based on Geertsma's poroelastic solution with nucleus of strain theory. The pressure profile is obtained by considering the critical transition time for transient and pseudo steady state flow. Then, the superposition principle is applied to calculate subsidence for the whole discretized model. The numerical model is first compared with Geertsma's analytical solution, which shows an excellent match. A comprehensive parametric study is performed to characterize the influence of different parameters. To show the applicability of the model for arbitrary shape reservoirs, a horizontal well with elliptical pressure depletion profile is created and the corresponding 3D land subsidence profile is obtained.

## 1. INTRODUCTION

The reservoir compacts due to fluid withdrawal by oil production. This process will finally lead to land subsidence in the surface if no proper water injection treatment is done. States like California, Texas, and Louisiana have suffered the damage for a long time (Pratt and Johnson 1926, Sinder 1927, Gilluly and Grant 1949, Chang et al. 2014). The first mathematical model for land subsidence was attempted by MacCann and Wilts to computing subsidence due to underground oil production (MacCann and Wilts 1951). They investigated two different models, which are "tension center" and "vertical pincer" model for the subsidence behavior above the Wilmington field. Based on their work, Geertsma improved the analogy between the physical parameters of the ground and those in the model using the nucleus-of-strain concept (Mindlin and Cheng 1950, Sen 1950, Geertsma 1973). Segall investigated the subsidence from the theoretical analysis, laboratory experimentation, and direct observation in the field (Segall 1992). The approach used by Segall was similar to Geertsma's approach, which derived the stress field and the surface subsidence resulting from the extraction of fluid or gas from the reservoir. Both of them considered the case of a uniform pressure depletion in a horizontal tabular reservoir and obtained identical solutions as well. Since then, most

subsidence studies were based on Segall and Geertsma's work (Fokker and Orlic 2006, Tempone et al. 2010, Chen 2011). On the other hand, the inversion technique which employs surface subsidence observations (GPS, radar, tiltmeter monitoring) can calculate reservoir behavior from subsidence behavior (Fokker 2002, Kroon et al. 2009, Fokker et al. 2012).

For numerical studies of land subsidence prediction, Morita developed a method to determine subsidence, compaction, and in-situ stress induced by pore-pressure change using a three-dimensional finite-element model (Morita et al. 1989). He found that Geertsma's results which are based on no modulus contrast between cap and reservoir rocks should be extended to simulate more realistic reservoirs to consider distinct property differences between the cap and reservoir rocks. However, the finite element modeling has an increased computational cost. Suzuki extended Geertsma's model to 3D shape reservoirs and 3D shape earth surface (Suzuki and Morita 2004).

This paper presents a numerical model based on Geertsma's poroelastic solution to calculate land subsidence due to oil production. No contrast in elastic properties between the reservoir and the surrounding formation is assumed. The superposition principle is applied to calculate subsidence for the whole discretized

model (Janssen 1981, Chan and Zoback 2007, Mallman and Zoback 2007). For constant pressure depletion case, the comparison between analytical solution and numerical results shows an excellent agreement, which indicates the model is capable of simulating more complex situations. The further case studies first consider non-uniform pressure depletion profiles due to different production histories. Then, cases with different compaction coefficient due to Poisson's ratio and Young's modulus change are simulated to characterize the influence of rock properties. Finally, a horizontal well with elliptical pressure depletion profile is created and the 3D land subsidence profile is obtained. The new approach can provide accurate subsidence profile and overcomes deficiencies in previous studies, which are uniform pressure drop and disk shape reservoir assumptions. This approach is also important for the future development of sound numerical models with multiple injection and production wells.

## 2. APPROACH

The surface subsidence is induced by underground compaction. The compaction equation is written as (Fjar et al. 2008)

$$\frac{\Delta h}{h} = C_m \alpha \Delta p \quad (1)$$

The compaction coefficient  $C_m$  is related to rock Poisson's ratio and Young's Modulus as

$$C_m = \frac{1}{E} \frac{(1+\nu)(1-2\nu)}{1-\nu} \quad (2)$$

The compaction is proportional to the pressure drop from Eq. (1). There are several analytical models used for subsidence characterization. In Geertsma's model the theory of "nucleus of strain" was employed as shown in Fig. 1. According to the theory, the vertical subsidence at any given radius  $r$  is

$$u_z(r, 0) = -\frac{1}{\pi} c_m (1-\nu) \frac{D}{(r^2 + D^2)^{\frac{3}{2}}} \Delta p V \quad (3)$$

Eq. (3) can be used to calculate subsidence at any point of interest (POI). The model was extended to deal with certain type of reservoir, i.e., disk shape reservoir. To get the subsidence, the solution is integrated over the whole reservoir area. The expression is (Geertsma 1973)

$$u_z(r, 0) = -2C_m(1-\nu)\Delta p h R \int_0^\infty e^{-D\alpha} J_1(\alpha R) J_0(\alpha r) d\alpha \quad (4)$$

Where  $J_0$  and  $J_1$  are Bessel functions of zero and first order, respectively. The subsidence can be obtained after integration. As we can see in Eq. 4, the average pressure drop in the reservoir is assumed. To model a more realistic situation, transient pressure distribution in reservoir is desired. During the early time of production, the reservoir is under infinite acting and the compaction can be neglected. After the period of infinite acting, the pressure

decline rate is constant, which results in pseudo steady state flow.

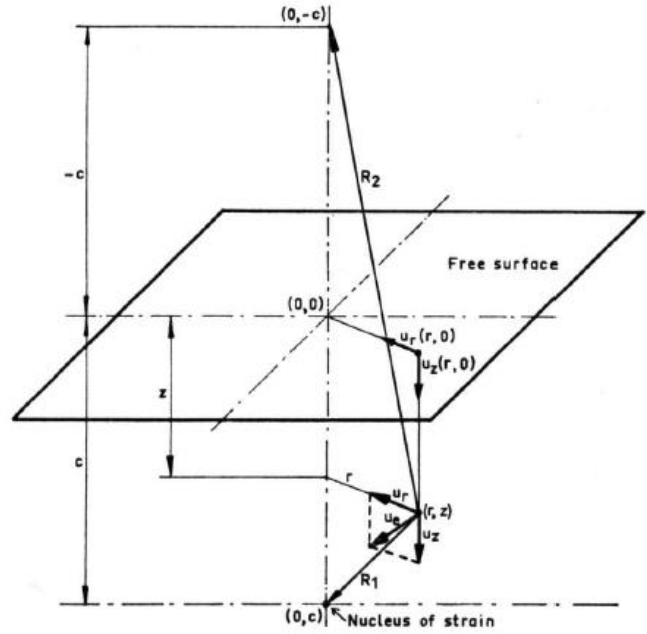


Fig. 1. Nucleus of strain (Geertsma 1966)

Fig. 2 shows the transient and pseudo steady state pressure profiles. To get the final pressure profile, a critical transition time from transient flow regime to pseudo steady state flow regime is obtained as (Dake 1978)

$$t_s = \frac{948\phi\mu c_t r_e^2}{k} \quad (5)$$

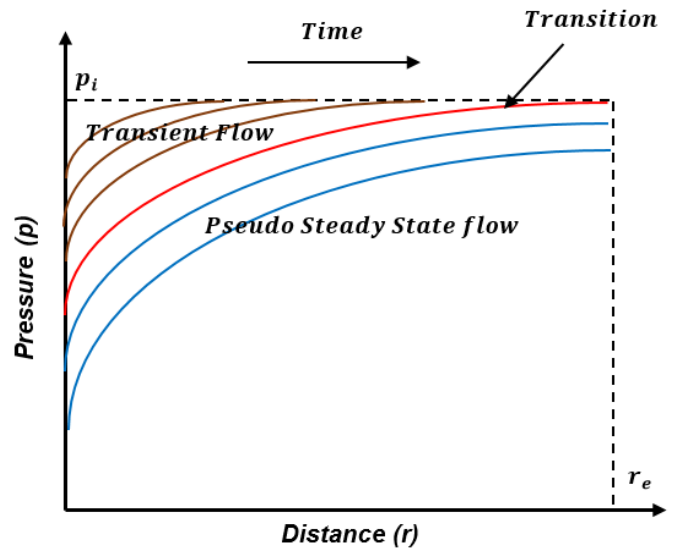


Fig. 2. Pressure profile of transient flow and pseudo steady state flow.

If time is less than  $t_s$ , the pressure distribution is

$$p(r, t) = p_i + 70.6 \frac{qB\mu}{kh} E_i \left( \frac{-948\phi\mu c_t r^2}{kt} \right) \quad (6)$$

If time is larger than  $t_s$ , the pressure is

$$p(r, t) = p_i - 141.2 \frac{qB\mu}{kh} \left[ \frac{0.000527kt}{\phi\mu c_t r_e^2} + \ln\left(\frac{r_e}{r_w}\right) - \frac{3}{4} \right] \quad (7)$$

With given reservoir and fluid properties, the final pressure profile can be obtained from Eq. (5)-(7).

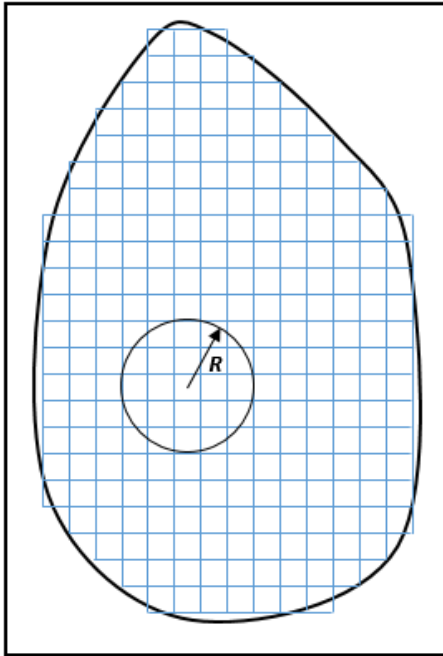


Fig. 3. Mesh of reservoir

After determining the pressure profile, the next step is to calculate the subsidence. Because of the non-uniform pressure drop, the reservoir is meshed with many blocks as shown in Fig. 3.

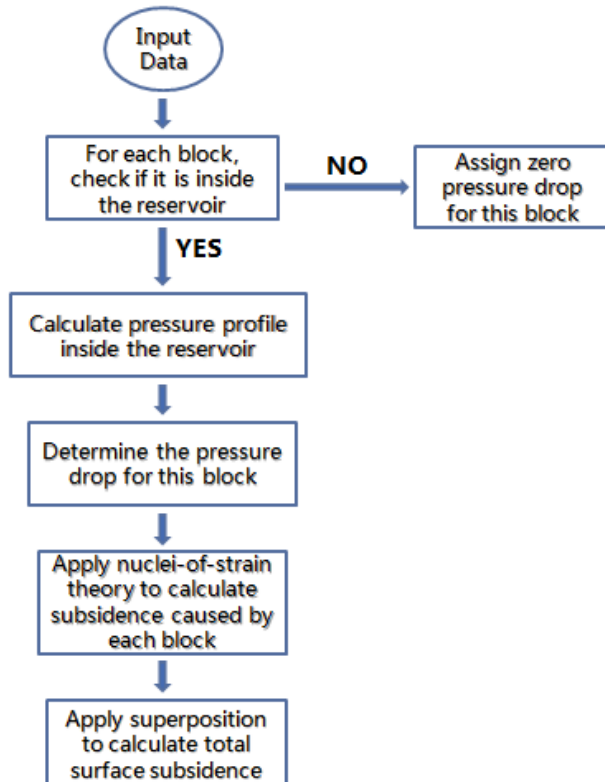


Fig. 4. Flow chart of the numerical model

Then, the subsidence of the whole field is calculated block by block. The principle of superposition is used to get the final subsidence for each block in the field.

Based on the approach described above, a flow chart for the numerical simulation is shown in Fig. 4. The first step is inputting reservoir and fluid properties for each block. Then, the next step is to assign pressure drop based on the pressure profile in the reservoir area. The nucleus of strain is performed for each reservoir block to calculate the subsidence. Finally the superposition principle is applied to calculate the total subsidence for the whole field.

### 3. RESULTS AND DISCUSSION

To evaluate the model, a case study is conducted to compare with Geertsma's analytical solution. Fig. 5 shows the pressure distribution of Geertsma's model and the numerical model. The uniform pressure profile and continuous pressure profile are used in Geertsma's model and our model, respectively. Both models have an average pressure drop of 2500 psi.

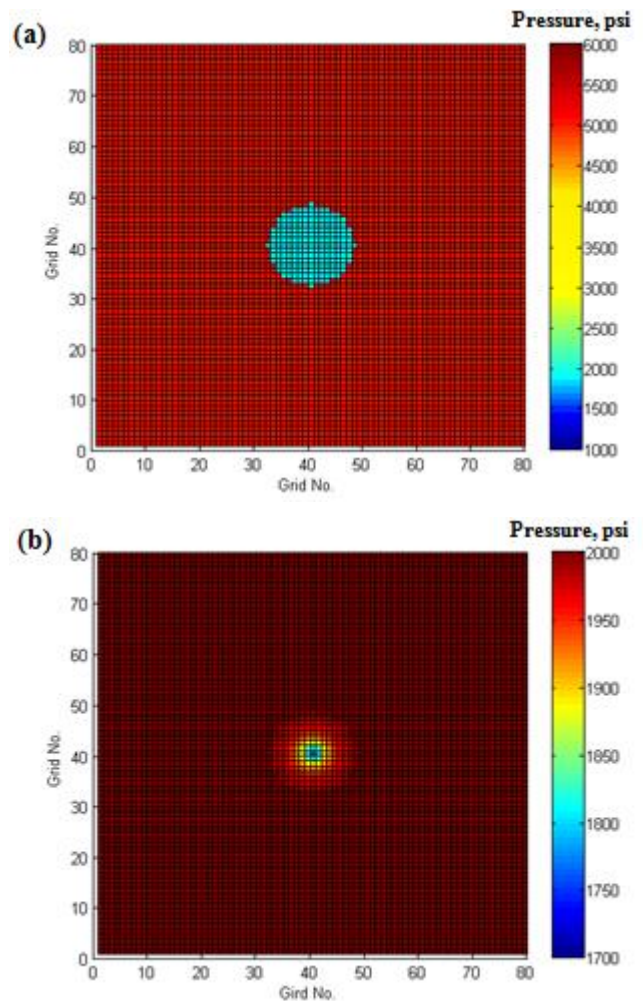


Fig. 5. Top view of pressure profile of (a) Geertsma's model. (b) The numerical model.

Parameters used in the simulation are shown in Table 1. Note that the initial reservoir pressure is 5000 psi and production rate is 100 STB/D.

Table 1. Parameters used in the simulation

Parameters	Value
Reservoir thickness, $h$	50 ft
Initial wellbore pressure, $p_i$	5000 psi
Oil formation volume factor, $B_o$	1.15 rb/stb
Reservoir radius, $r_e$	5000 ft
Oil production, $q$	100 STB/D
Oil viscosity, $\mu$	2 cp
Total compressibility, $C_t$	$1e-5 \text{ psi}^{-1}$
Reservoir diameter, $D$	5000 ft
Permeability, $k$	50 md
Wellbore radius, $r_w$	0.5 ft
Poisson's ratio, $\nu$	0.25
Young's Modulus, $E$	2 Gpa
Production time, $t$	20 years

The subsidence results are shown in Fig. 6. The subsidence profile is perfectly matched with Geertsma's analytical solution. The deepest subsidence is about 0.035 ft after 20 years production. Thus, the numerical model using the superposition principle is valid. However, the numerical model is more accurate for actual oil production since the continuous pressure drop is considered and the subsidence outside of the reservoir can be obtained.

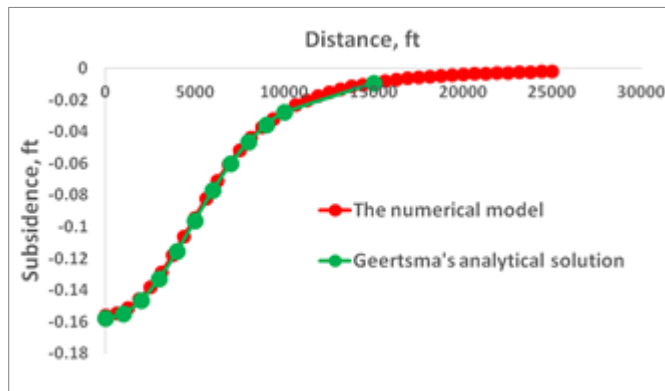


Fig. 6. Comparison of Geertsma's model and the numerical model.

From Eq. (3) and (7), it can be seen that different parameters can affect the subsidence. To do parametric analysis of subsidence, the production rate, production time, Poisson's ratio, Young's Modulus and reservoir thickness are considered.

**Production rate.** To characterize the influence of production rate on the subsidence, three cases are created with 50 STB/D, 100 STB/D and 150 STB/D production. In these cases, all other parameters are kept unchanged except the production rate. The pressure profiles are shown in Fig. 7 (a)-(c). The X axis shows the grid No. in the reservoir and Y axis shows the pressure for that block. The lowest pressure occurs at the reservoir center (grid No. 40). Note that the color of pressure distribution corresponds to the reservoir pressure on the Y axis.

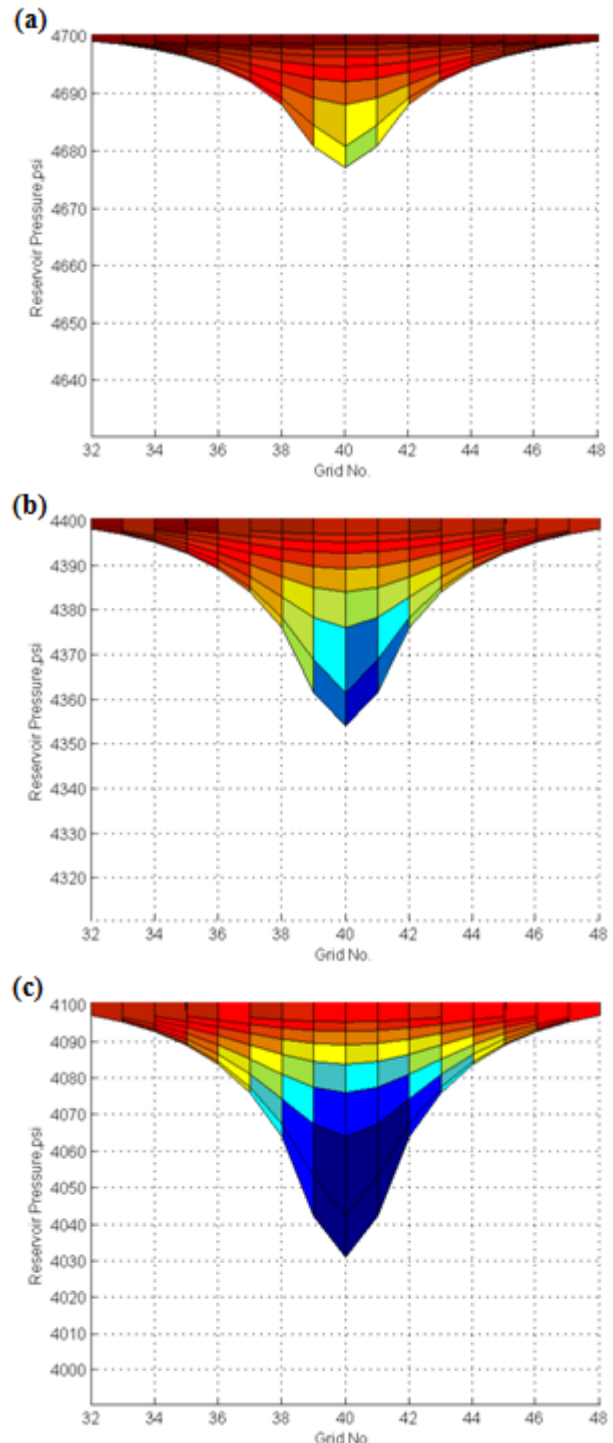


Fig. 7. (a) Pressure profile of case  $q=50$  STB/D. (b) Pressure profile of case  $q=100$  STB/D. (c) Pressure profile of case  $q=150$  STB/D.

With the production rate increasing from 50 STB/D to 150 STB/D, the pressure in the reservoir center decreases from 4678 psi to 4032 psi. The pressure difference can be explained by Eq. (7) since the pressure has an inverse relationship with the production rate.

The subsidence profiles are shown in Fig 8 (a)-(c). The subsidence has parabolic profile with negligible subsidence on the boundaries. The deepest subsidence increases from 0.02 ft to 0.058 ft in the reservoir center, which corresponds to the location of largest pressure depletion.

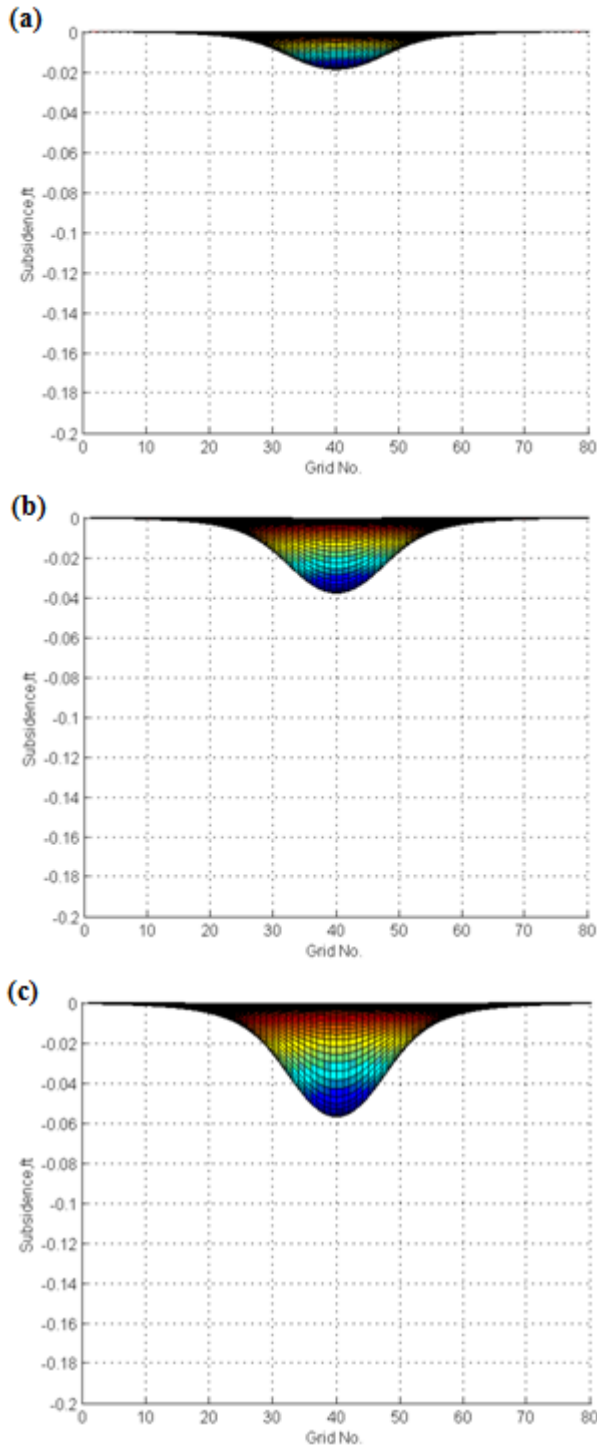


Fig. 8. (a) Subsidence of case  $q=50$  STB/D. (b) Subsidence of case  $q=100$  STB/D. (c) Subsidence of case  $q=150$  STB/D.

**Production time.** Similarly, three cases with production time of 10 years, 20 years and 30 years are created to characterize the influence of production time. Pressure profiles are shown in Figure 9 (a)-(c). If the production time increases from 10 years to 30 years, the pressure in the reservoir center decreases from 4655 psi to 4055 psi, which means that the reservoir pressure has an inverse relationship with the production time.

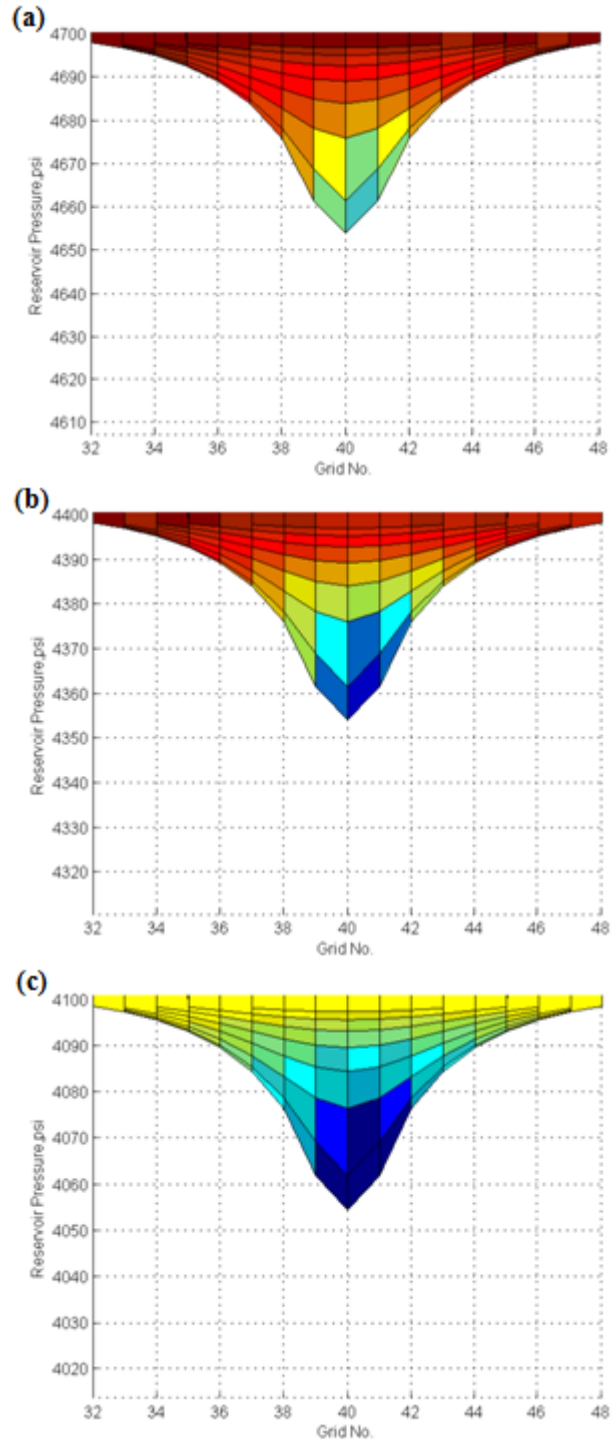


Fig. 9. (a) Pressure profile of case  $t=10$  years. (b) Pressure profile of case  $t=20$  years. (c) Pressure profile of case  $t=30$  years.

The subsidence profiles of these three cases are shown in Fig. 10 (a)-(c). The deepest subsidence increases from

0.02 ft to 0.057 ft in the reservoir center, which has the similar trend as the pressure depletion.

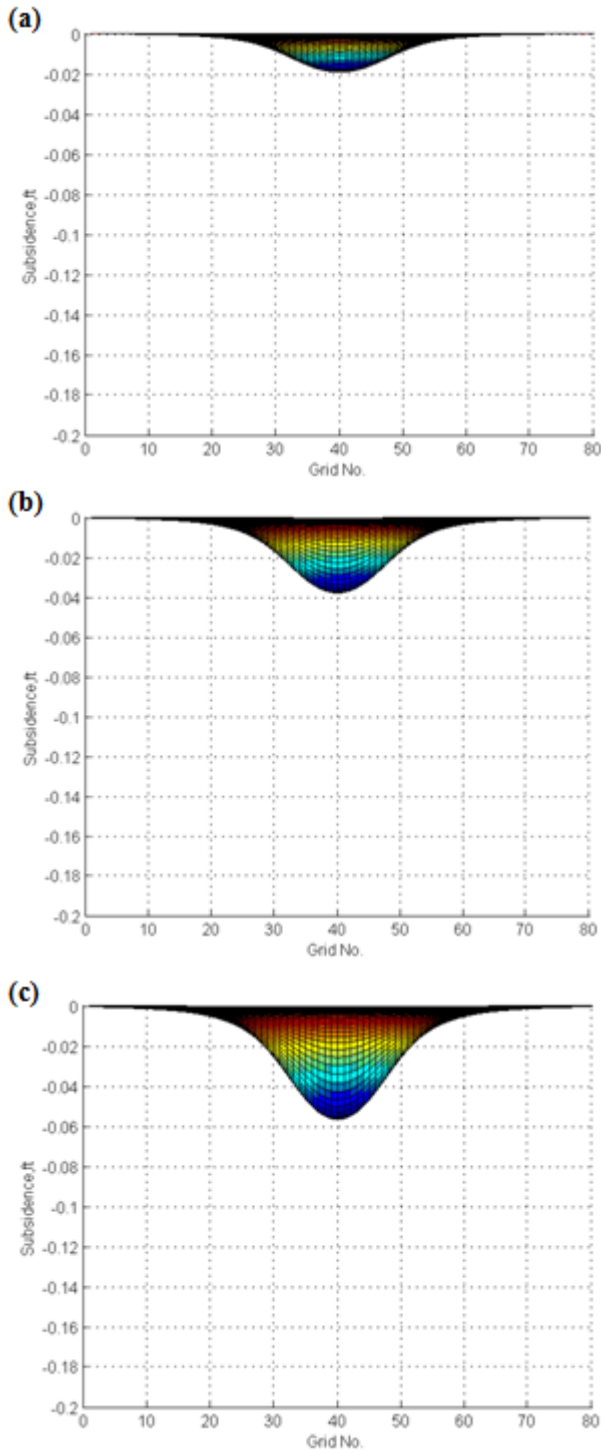


Fig. 10. (a) Subsidence of case  $t=10$  years. (b) Subsidence of case  $t=20$  years. (c) Subsidence of case  $t=30$  years.

**Poisson's ratio.** In this section, three cases with Poisson's ratio (both the reservoir and surrounding formation) of 0.125, 0.25 and 0.375 are simulated. The pressure profiles are the same as Fig. 7 (b) because Poisson's ratio does not affect the pressure distribution from Eq. (7).

However, Poisson's ratio can affect the subsidence profile. The subsidence profiles are shown in Fig. 11 (a)-(c). The

subsidence decreases as Poisson's ratio increases. The reason is that the compaction coefficient has an inverse relationship with Poisson's ratio as expressed in Eq. (2). Therefore, the final subsidence has an inverse relationship with Poisson's ratio.

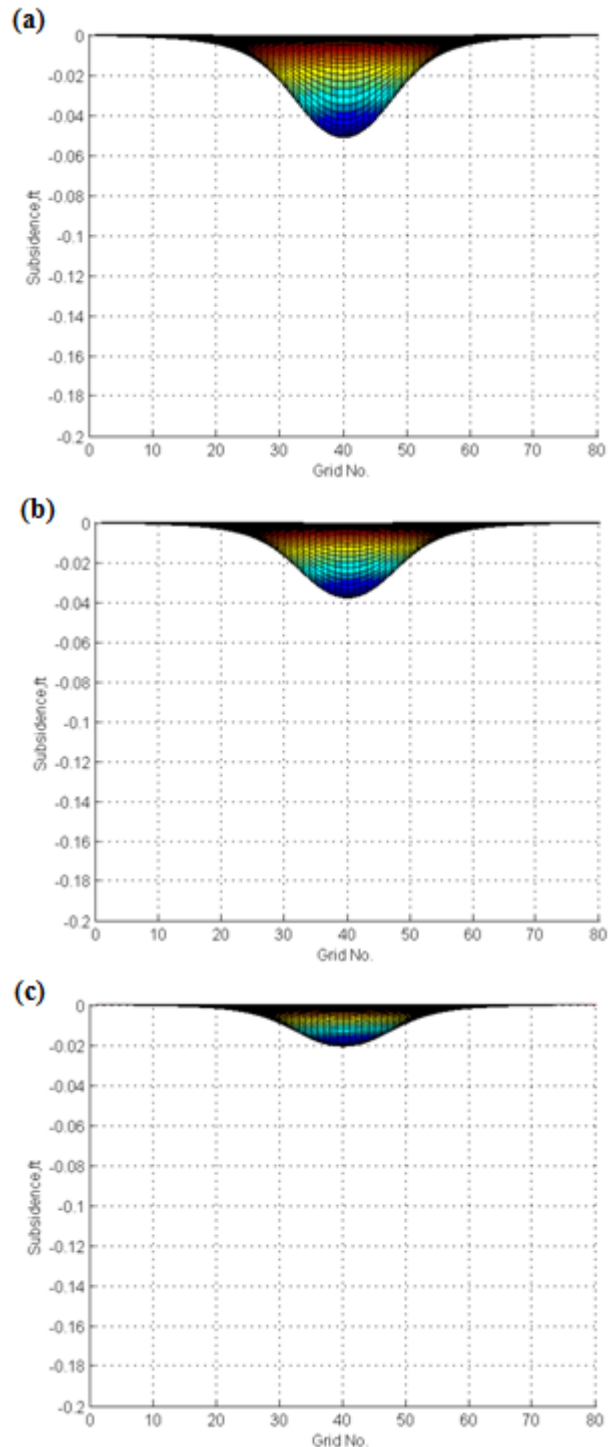


Fig. 11. (a) Subsidence of case  $\nu=0.125$ . (b) Subsidence of case  $\nu=0.25$ . (c) Subsidence of case  $\nu=0.375$ .

**Young's modulus.** Another important rock property is Young's modulus. Three cases with Young's modulus (both the reservoir and surrounding formation) of 1 Gpa, 2 Gpa and 3 Gpa are performed. The pressure profiles are

also the same as Fig. 7 (b) because Young's modulus does not affect the pressure depletion.

The subsidence profiles are shown in Fig. 12 (a)-(c). Similar to Poisson's ratio influence, the subsidence has an inverse relationship with Young's modulus. The increase of Young's modulus results in the reduction of subsidence.

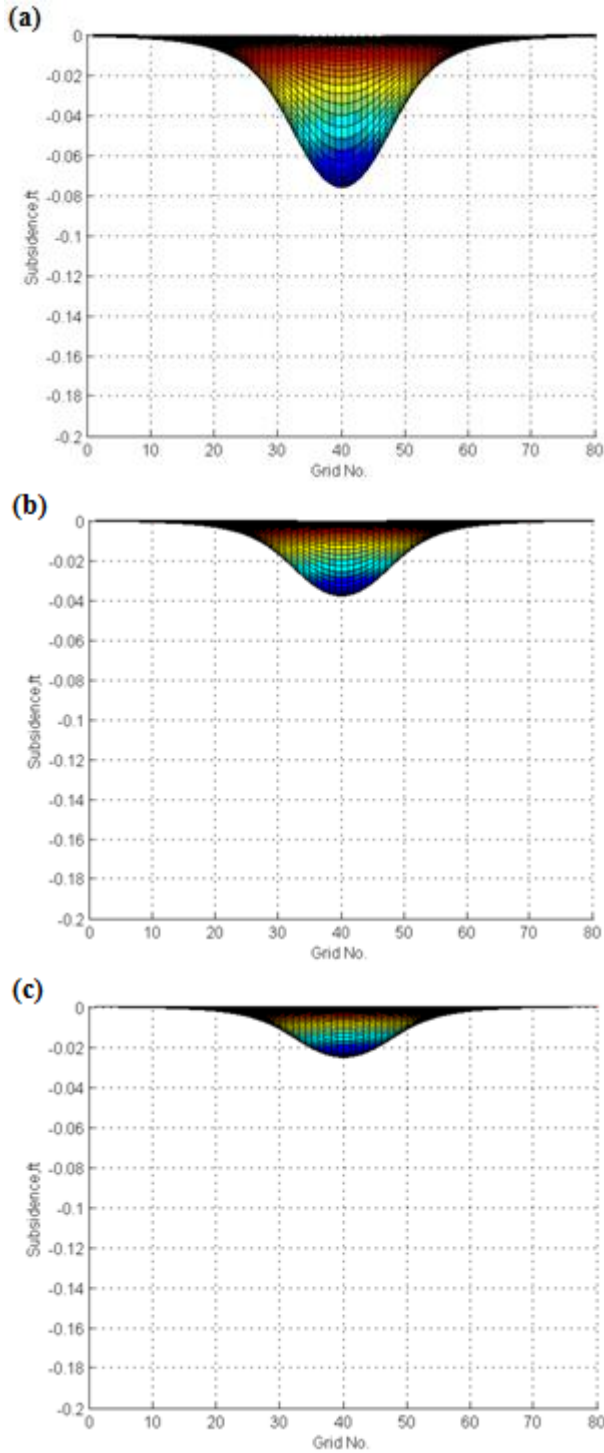


Fig. 12. (a) Subsidence of case  $E=1$  Gpa. (b) Subsidence of case  $E=2$  Gpa. (c) Subsidence of case  $E=3$  Gpa.

**Reservoir thickness.** Three cases with reservoir thickness of 25 ft, 50 ft and 75 ft are conducted in this section. The pressure profiles are shown in Fig. 13 (a)-(c).

The smaller reservoir thickness causes larger pressure depletion because 25 ft case has the largest pressure depletion as shown in the figure. So the pressure has an inverse relationship with the reservoir thickness.

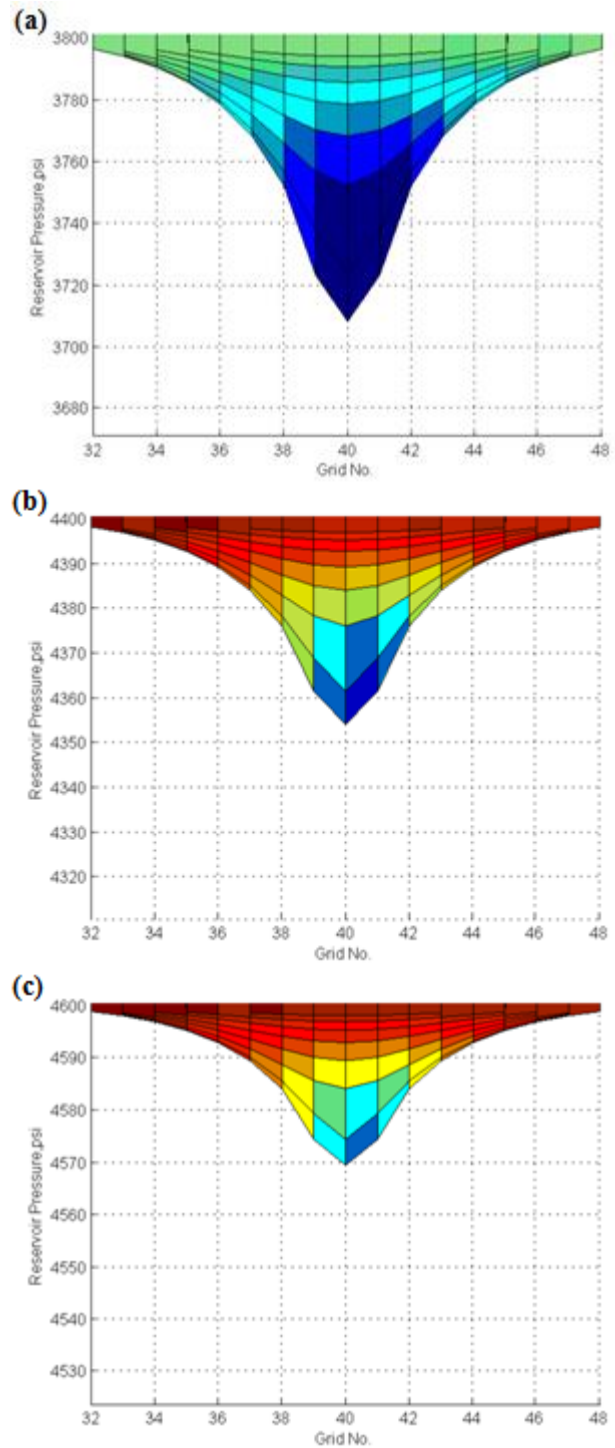


Fig. 13. (a) Pressure profile of case  $h=25$  ft. (b) Pressure profile of case  $h=50$  ft. (c) Pressure profile of case  $h=75$  ft.

However, the subsidence profiles for three cases are the same as shown in Fig. 14 (a)-(c). The deepest subsidence is constant about 0.038 ft. The reservoir thickness can affect both the pressure distribution equation (Eq. (7)) and nucleus of strain equation (Eq. (3)). But the reservoir thickness will be cancelled out when combining these two

equations. So given a constant production rate, reservoir thickness does not affect subsidence.

For reservoir thickness, it has no effect on the subsidence but it can affect the pressure profile.

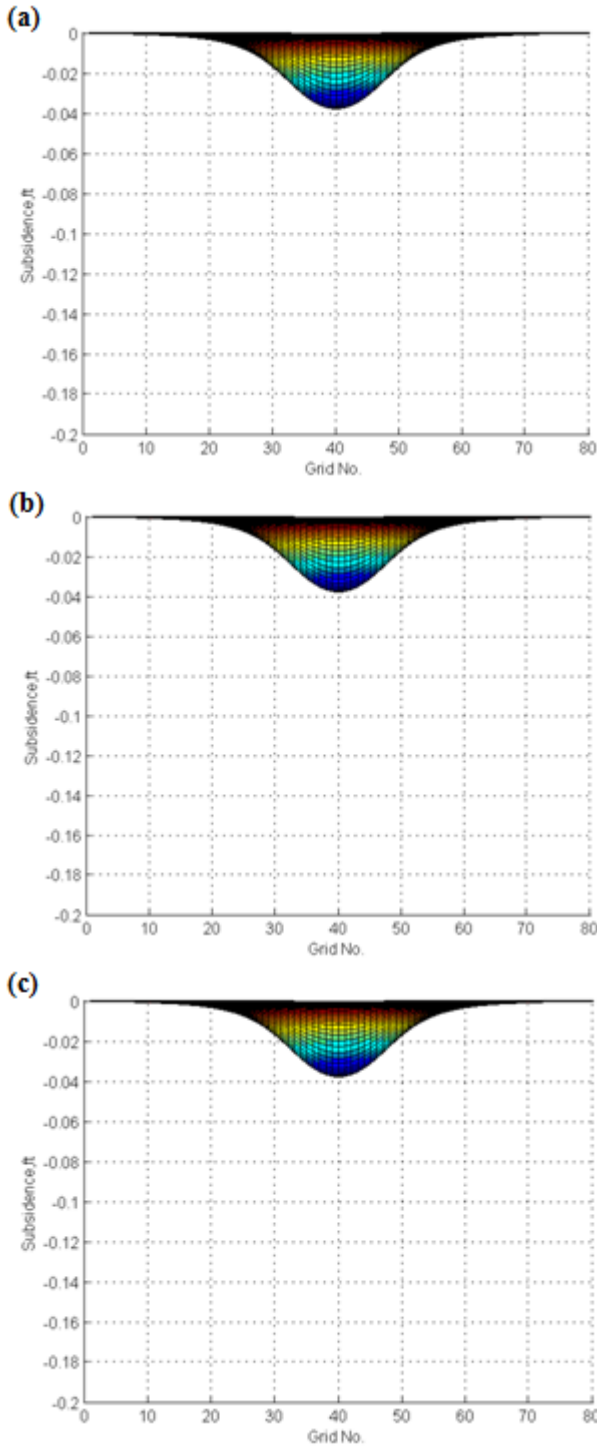


Fig. 14. (a) Subsidence of case  $h=25$  ft. (b) Subsidence of case  $h=50$  ft. (c) Subsidence of case  $h=75$  ft.

To quantify the influence of each parameter, a tornado diagram is created based on the previous results. As shown in Fig. 15, the production rate and production time have similar influence on the subsidence. Poisson’s ratio has medium effect on the subsidence. Young’s modulus can affect the subsidence a lot for decreasing case because it has a linear relationship with the compaction coefficient.

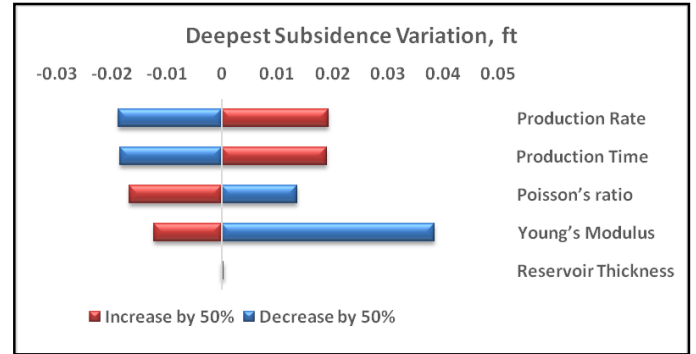


Fig. 15. Tornado diagram of deepest subsidence variance

**Horizontal well case.** A significant advantage of the numerical model is the capability to calculate subsidence for any shape of reservoir without complex integrals. A horizontal well case is performed. Assume that the well has an elliptical shape of pressure drop profile as shown in Fig. 16. The largest pressure drop is 3500 psi along the well path and the pressure drop gradually decreases to 500 psi on the boundaries.

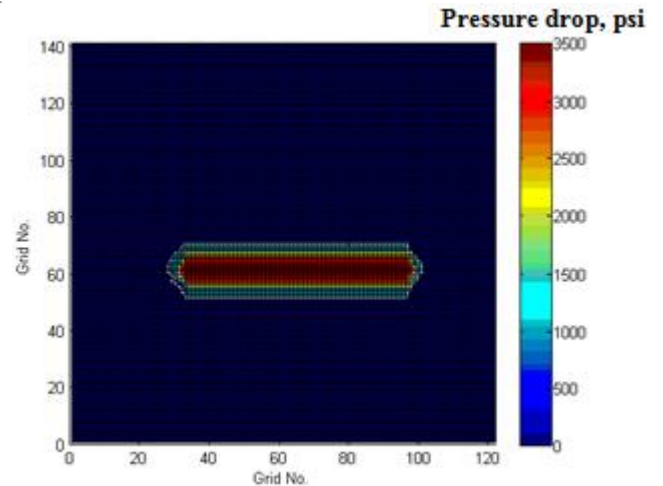


Fig. 16. Top view of the pressure drop profile for horizontal well case.

The 2D top view of subsidence profile is shown in Fig. 17. The subsidence distribution is similar to pressure drop distribution, which validates the relationship between the pressure drop and the subsidence in Eq. 3.

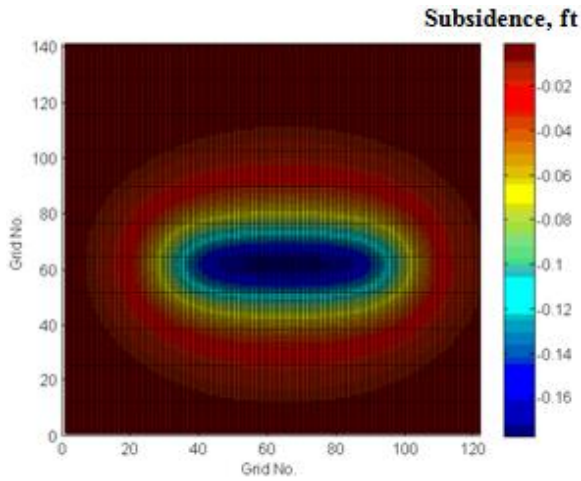


Fig. 17. 2D top view of subsidence for horizontal well case.

For better observation, 2D and 3D side views of subsidence are shown in Fig. 18. The subsidence profiles are in accordance with our expectations. The severest subsidence point can be detected based on the subsidence profile.

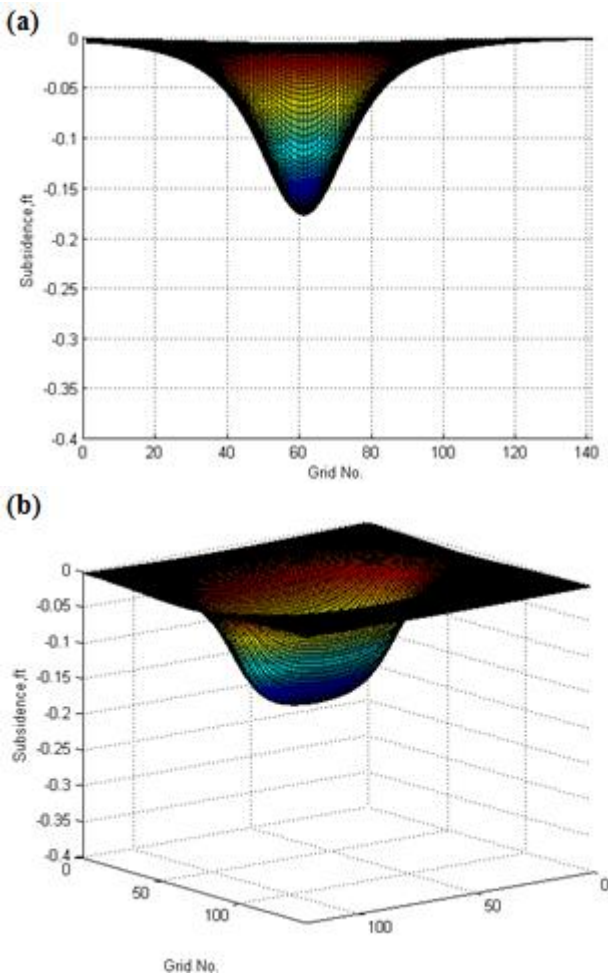


Fig. 18. Horizontal well subsidence. (a) 2D side view. (b) 3D side view.

#### 4. CONCLUSIONS

In this paper, a numerical model has been developed for subsidence prediction and a parametric study has been performed. It was found that the subsidence has a positive relationship with production rate and time and an inverse relationship with Poisson's ratio and Young's modulus. The reservoir thickness does not affect the subsidence for a given production rate. For the disk-shape reservoir, the results are reasonable and close to Geertsma's analytical model (uniform pressure drop). The model is capable to calculate subsidence of any shape of reservoirs with known pressure drop distribution. For the future work, subsidence prediction can be achieved by switching the depth of each block from a constant value to a variable for inclined reservoirs. The numerical model can also be used for the future development of sound numerical models with multiple injection and production wells.

#### NOMENCLATURE

$h$	Reservoir thickness, ft
$\Delta h$	Reservoir compaction height, ft
$C_m$	Compaction coefficient, $\text{psi}^{-1}$
$\alpha$	Biot's coefficient
$E$	Young's modulus, psi
$\nu$	Poisson's ratio
$u_z$	Vertical subsidence, ft
$D$	Reservoir diameter, ft
$r$	Distance, ft
$\Delta p$	Pressure drop, psi
$V$	Reservoir volume, $\text{ft}^3$
$R$	Radius distance from vertical axis, ft
$t_s$	Critical transition time, hours
$K$	Permeability, md
$\phi$	Porosity
$C_t$	Total compressibility, $\text{psi}^{-1}$
$r_e$	Reservoir radius, ft
$\mu$	Viscosity, cp
$p_i$	Initial reservoir pressure, psi
$p$	Wellbore pressure, psi
$t$	Production time, hours
$B$	Oil formation volume factor, rb/stb
$q$	Production rate, STB/D
$r_w$	Wellbore radius, ft

## REFERENCES

1. Chan, A. and Zoback, M. 2007. The role of hydrocarbon production on land subsidence and fault reactivation in the Louisiana coastal zone. *Journal of Coastal Research*, volume 23, issue 3, 771-786.
2. Chen, Z. 2011. Poroelastic model for induced stresses and deformations in hydrocarbon and geothermal reservoirs. Volume 80, Issue 1, 41-52.
3. Chang, C. et al. 2014. Time-dependent subsidence associated with drainage-induced compaction in Gulf of Mexico shales bounding a severely depleted gas reservoir. *AAPG Bulletin*, v.98, No.6, 1145-1159.
4. Dake, L.P. 1978. *Fundamentals of reservoir engineering*. Elsevier Science B.V., Netherland.
5. Fjar, E. et al. 2008. *Petroleum related rock mechanics*. 2nd Edition, Elsevier 2. Chapter 12.
6. Fokker, P. and Orlic, B. 2006. Semi-analytic modeling of subsidence. *Mathematical Geology*, Volume 38, NO. 5, 565-589.
7. Fokker, P. 2002. Subsidence prediction and inversion of subsidence data. *SPE/ISRM paper 78227*.
8. Fokker, P. et al. 2012. Inversion of surface subsidence data to quantify reservoir compartmentalization: a field study. *Journal of Petroleum Science and Engineering*, 96-97, 10-21.
9. Geertsma, J. 1973. Land subsidence above compacting oil and gas reservoir. *Journal of Petroleum Technology*, volume 25, issue 06, 734-744.
10. Geertsma, J. 1966. Problems of rock mechanics in petroleum production engineering. *Proc., 1<sup>st</sup> Congress of the Intl. Soc. Of Rock Mech., Lisbon, I, 585-594*.
11. Gilluly, J. and Grant, U. 1949. Subsidence in the Long Beach Harbor area, California. *Bull., GSA, 60, 461*.
12. Janssen, J. 1981. A computer program for predicting surface subsidence resulting from pressure depletion in geopressured wells: subsidence prediction for the Dow test well NO. 1, Parcperdue, Louisiana. *Fifth Conference: Geopressured-Geothermal Energy. 281-284*.
13. Kroon, I. et al. 2009. Disentangling shallow and deep processes causing surface movement. *Mathematical Geosciences*, 41, 571-584.
14. Mallman, E. and Zoback, M. 2007. Subsidence in the Louisiana coastal zone due to hydrocarbon production. *Journal of Coastal Research*, Special issue 50.
15. McCann, G.D. and Wilts, C.H. 1951. A mathematical analysis of the subsidence in the Long Beach-San Pedro area. *Internal report, California Institute of Technology*.
16. Mindlin, R.D. and Cheng, D.H. 1950. Thermo-elastic stress in the semi-infinite solid. *J. Applied Phys., 21, 931*.
17. Morita, N. et al. 1989. A quick method to determine subsidence, reservoir compaction, and in-situ stress induced by reservoir depletion. *SPE paper 17150-PA*.
18. Pratt, W. and Johnson D. 1926. Local subsidence of the Goose Creek oil field. *Journal Geology. Volume 34, Number 7*.
19. Segall, P. 1992. Induced stresses due to fluid extraction from axisymmetrical reservoirs. *Pure and applied geophysics*, volume 139, issue 3, 535-560.
20. Sen, B. 1950. Note on the stress produced by nuclei of thermoelastic strain in a semi-infinite elastic solid. *Quarterly Applied Math, 8, 635*.
21. Snider, L. 1927. A suggested explanation for the surface subsidence in the Goose Creek oil and gas field, Texas. *AAPG, 11, 729*.
22. Suzuki, I. and Morita, N. 2004. Subsidence and horizontal earth surface movement during reservoir depletion for 3D reservoirs with 3D earth surface. *SPE paper 89960-MS*.
23. Tempone, P. et al. 2010. Improved solution of displacements due to a compacting reservoir over a rigid basement. *Applied Mathematical Modeling, 34, 3352-3362*.